Positive trend in the mean speed and deformation rate of Arctic sea ice, 1979–2007

P. Rampal,[1,2] J. Weiss,[1] and D. Marsan[2]

Received 1 August 2008; revised 25 February 2009; accepted 11 March 2009; published 14 May 2009.

[1] Using buoy data from the International Arctic Buoy Program, we found that the sea ice mean speed has substantially increased over the last 29 years (+17% per decade for winter and +8.5% for summer). A strong seasonal dependence of the mean speed is also revealed, with a maximum in October and a minimum in April. The sea ice mean strain rate also increased significantly over the period (+51% per decade for winter and +52% for summer). We check that these increases in both sea ice mean speed and deformation rate are unlikely to be consequences of a stronger atmospheric forcing. Instead, they suggest that sea ice kinematics play a fundamental role in the albedo feedback loop and sea ice decline: increasing deformation means stronger fracturing, hence more lead opening, and therefore a decreasing albedo. This accelerates sea ice thinning in summer and delays refreezing in early winter, therefore decreasing the mechanical strength of the cover and allowing even more fracturing, larger drifting speed and deformation, and possibly a faster export of sea ice through the Fram Strait. The September minimum sea ice extent of 2007 might be a good illustration of this interplay between sea ice deformation and sea ice shrinking, as we found that for both winter 2007 and summer 2007 exceptionally large deformation rates affected the Arctic sea ice cover.

Citation: Rampal, P., J. Weiss, and D. Marsan (2009), Positive trend in the mean speed and deformation rate of Arctic sea ice, 1979–2007, *J. Geophys. Res.*, *114*, C05013, doi:10.1029/2008JC005066.

1. Introduction

[2] The Arctic sea ice cover can be considered as a thin plate stressed mainly under the action of winds and ocean currents [*Thorndike and Colony*, 1982]. This leads to the fracturing and faulting of the sea ice cover, which accommodate most of its deformation [*Schulson*, 2004; *Weiss et al.*, 2007]. This process, along with thermodynamics, controls the amount of open water, the ice thickness distribution, and indirectly the drifting properties of the sea ice cover. Consequently, sea ice kinematics is important for understanding the momentum, mass, and energy balance in the Arctic and more generally its influence on the Earth's climate [*Moritz et al.*, 2002]. For example, an increase of the drifting speed would suggest a larger amount of perennial sea ice exported through the Fram Strait [*Zhang et al.*, 2000; *Kwok and Rothrock*, 1999], then a relative increase of first-year sea ice in the basin, and consequently a thinning of the sea ice cover. Excepting the Fram, Banks and Nares straits, and the Barents Sea, the Arctic sea ice cover is essentially enclosed in a confined basin. Therefore, an increase of the mean drifting speed would suggest an increase of the strain rate, i.e., a stronger fracturing/faulting. This implies more lead opening, as well as an higher variability of the ice thickness, causing a decrease in the albedo and allowing more shortwave absorption by the ocean, thereby shrinking the cover during summer, reducing its strength, and increasing again the fracturing and faulting [*Zhang et al.*, 2000; *Moritz et al.*, 2002; *Kwok*, 2006]. On the other hand, fracturing during winter enhances the thermodynamically driven production of new ice, a negative feedback, and consequently modifies the heat and salinity budget in the Arctic Ocean [*Maykut*, 1982; *Alam and Curry*, 1997; *Lüpkes et al.*, 2008]. These complex processes are highly nonlinear and need to be investigated in more details to understand their role in the Arctic sea ice decline and more generally on climate change. Thirty years ago, the Arctic sea ice cover extended on average over about 14 million km^2 at the end of winter and 7 million km^2 at the end of summer. There is now consensus toward a significant shrinking during the last decades, both in terms of spatial extension and average thickness [*Lemke et al.*, 2006], supposedly mainly under the action of thermodynamic processes, although recent works suggested that the flushing of thick, multiyear ice out through Fram Strait could be a significant cause of sea ice mass loss [*Lindsay and Zhang*, 2005]. A spectacular illustration was recently given during the 2007 melt season, as the perennial sea ice further plummeted to the lowest levels since satellite measurements began in 1979. The average sea ice extent for September 2007 was 4.28 million km^2, the lowest on record, shattering the previous record, set in 2005, by

[1] Laboratoire de Glaciologie et Géophysique de l'Environnement, UMR5183, Université Joseph Fourier, CNRS, Saint Martin d'Hères, France.

[2] Laboratoire de Géophysique Interne et Tectonophysique, UMR5559, Université de Savoie, CNRS, Le Bourget du Lac, France.

0148-0227/09/2008JC005066

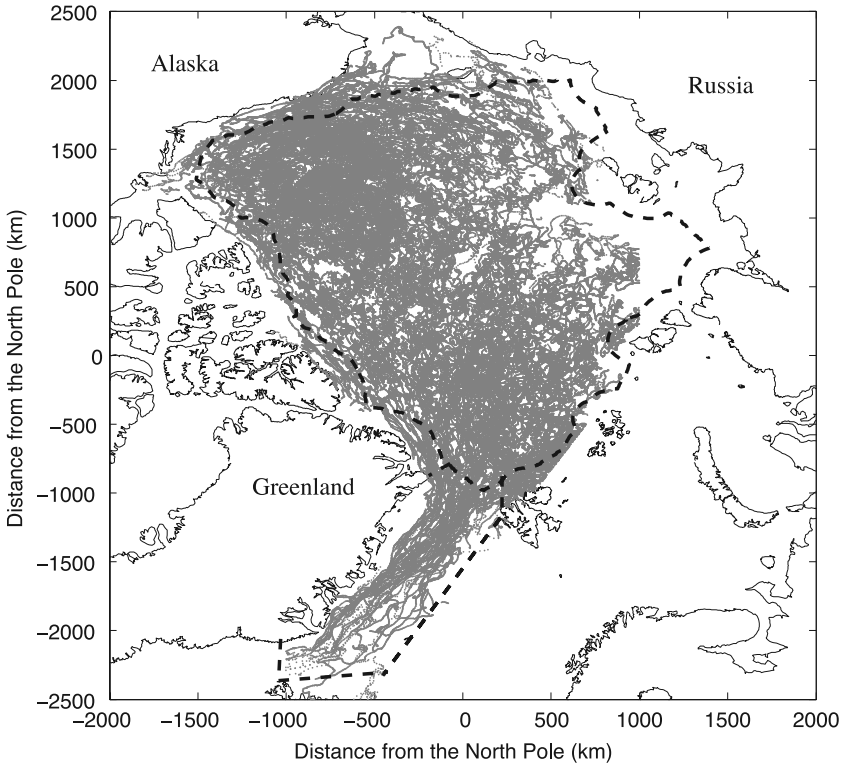

Figure 1. Map of the Arctic basin showing the buoys trajectories of the IABP data set, combining the 3 hourly data set of 1979–2001 and the 12 hourly data set of 2002–2007. The tracks have been recorded between January 1979 and December 2007. Only the Laptev Sea is poorly covered by this data set. In our study, we only used the IABP data that lie in the central Arctic (see the region delimited by the bold dashed line).

23%. September 2007 sea ice was 39% below the long-term average from 1979 to 2000. The September rate of sea ice decline since 1979 is now approximately 10% per decade, or 72,000 km^2 a^{-1}, a rate systematically underestimated by climate models [*Stroeve et al.*, 2007; *Serreze et al.*, 2007].

[3] On the other hand, *Lemke et al.* [2006] concluded that "There is no indication of long-term trend" in either ice motion, or ice export out of the Arctic basin. The results reported here reveal a different picture. As a revealing example, the drifting speed underwent in 2006–2007 by the polar schooner Tara was twice as large as the mean drifting speed of the Fram ship 115 years ago [*Gascard et al.*, 2008]. Tara drifted along the transpolar drift and reached the open ocean through Fram strait in late January 2008, i.e., 1 year earlier than expected by scientists. This motivated the present statistical study of the Arctic sea ice drifting speed and deformation rate evolutions over the last decades to evaluate a possible role of dynamic processes in the reduction of sea ice extent and thickness and the acceleration of its decline as observed in recent years.

[4] Our paper is organized as follow: First, we study the evolution of the mean speed of buoys that drifted according to the sea ice motion over the period 1979–2007 (section 3). Then, we check that the linear trends we obtained are statistically representative of a similar evolution of the whole Arctic sea ice motion (section 4). Second we study the time evolution of the sea ice cover deformation rates over the same period (section 5). Possible causes for the observed trends are then discussed in section 6.

2. Data Set

[5] We use the International Arctic Buoy Program (IABP) data set (available on the Web at ftp://iabp.apl.washington.edu/pub/IABP/C) that consists, from December 1978 to December 2001, of 3 hourly buoy positions, and from January 2002 to December 2007, of 12 hourly positions. These buoys are fixed on the ice and drift according to the ice motion. Errors on the positions range from 100m to 300m, depending on the type of the positioning system embarked on the buoy [*Thomas*, 1999]. We note here that the buoy positions distributed by the IABP differ slightly from the raw positions sampled by the buoys: The raw buoy's tracks were irregularly sampled through time, with a mean time interval of 1 h. The 3 hourly and 12 hourly positions are both issued from the same process: a cubic least squares fit of the raw positions was first performed before a resampling at 3- and 12-h time intervals, respectively (see the IABP documentation for further details). Figure 1 shows all the buoys tracks and some delimited regions (see below for further details). The reference coordinate system used in this study is a Cartesian coordinate system centered on the North Pole with the y axis following the Greenwich meridian. Each latitude-longitude buoy position is defined in the orthogonal base ($\mathbf{e}_1$, $\mathbf{e}_2$) of this

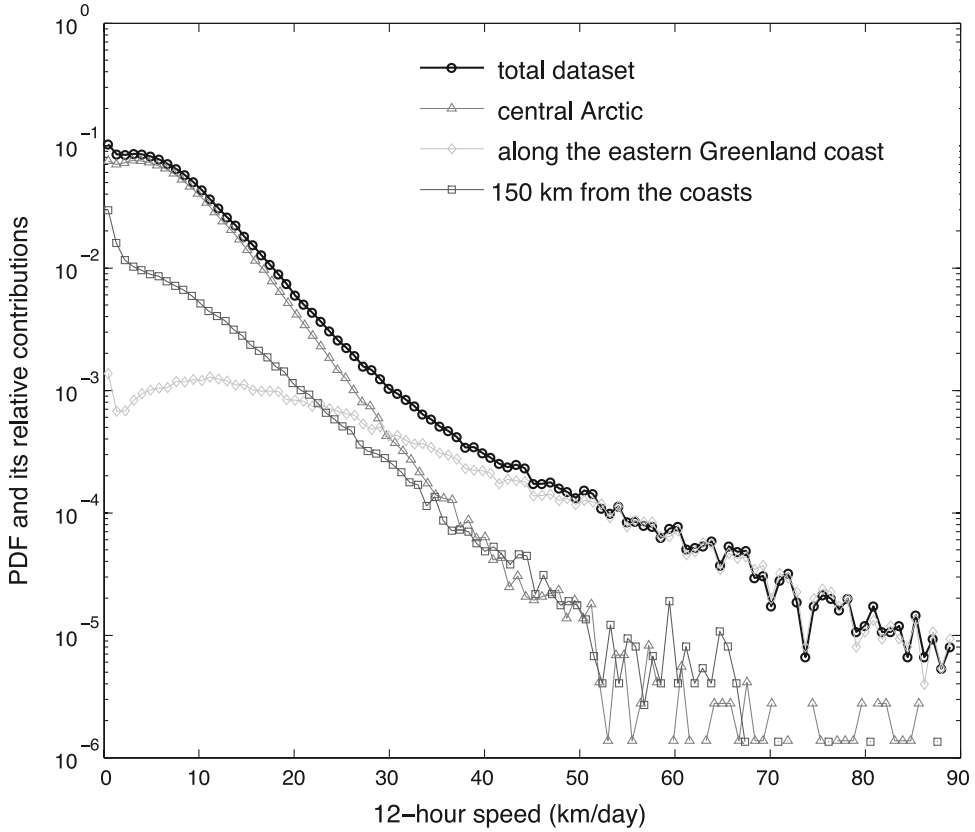

Figure 2. Probability density function of the 12-h speeds computed from the total IABP data set and its contributions coming from the regions drawn in Figure 1.

coordinate system as $\mathbf{x}_{(lat,lon)} = x\mathbf{e}_1 + y\mathbf{e}_2$ using a polar stereographic projection. In order to analyze a homogeneous data set, we work on 12-h displacements: For any given buoy position (x, y) of both 3 hourly and 12 hourly data sets, we compute the speeds $u_x\ (\tilde{x}, \tilde{t}) = (x(t + 12h) - x(t))/12h$ (along the x axis) and $u_y\ (\tilde{y}, \tilde{t}) = (y(t + 12h) - y(t))/12h$ (along the y axis) at all available times t, i.e., such that these exist recorded positions both at times t and $t + 12h$. Here, $\tilde{x}$, $\tilde{y}$, and $\tilde{t}$ are defined as the means $\tilde{x} = (x(t + 12h) + x(t))/2$, $\tilde{y} = (y(t + 12h) + y(t))/2$ and $\tilde{t} = ((t + 12h) + t)/2$. Given an error on raw positions ranging between 100 m and 300 m, the upper bound uncertainty on the 12-h speeds ranges from 0.3 to 0.9 km d^{-1}. The statistics on speed are sensitive to the scale over which the speed is computed, here set to 12 h. However, the Lagrangian correlation time for sea ice diffusion is typically of the order of a few days (5 days according to *Colony and Thorndike* [1984]; see also *Thorndike* [1986, Figure 6]). For all timescales below this Lagrangian time, a Lagrangian speed can be defined unambiguously [*Taylor*, 1921]. Table 1 recapitulates the number of buoys and the number of speed values per year, distinguishing winter from summer. For each season, the number of trajectories that were used in our analysis is also given. Figure 2 displays the probability density function (PDF) of the speed u defined as $u = (u_x^2 + u_y^2)^{(1/2)}$, for the entire data set. The contribution of the Fram Strait (see the corresponding region on the map of Figure 1), which is characterized by a strong southward advection of sea ice, is singled out. Almost all the speed values stronger than 50 km d^{-1} are recorded in the Fram Strait. Similarly, we single out the contribution of the buoy positions that lie within 150 km of a coast (see the map of Figure 1). These speeds are on average less than those of the central Arctic (see the map of Figure 1). We therefore decided to perform our analysis only on the Central Arctic data set. By doing so, we avoid biasing our statistics by the low speed values of fast ice. The Fram Strait region is also of particular interest, but the amount of data from the IABP data set does not allow us to perform an analysis with significant results for this region. In order to study this zone, we used the satellite derived velocity estimates provided by the Jet Propulsion Laboratory (see section 6).

3. Analysis of the Time Variation of Buoy Speed

3.1. Monthly Averages of Buoy Speed

[6] We here analyze whether the mean speed of the IABP buoys has changed over the last 3 decades. We will study in section 4 how these changes in buoy speed can potentially reflect underlying speed changes of sea ice, by examining spatial and temporal sampling issues inherent to buoy measurements. The mean speed over all buoys in the region, denoted $\overline{u}$, is here defined as the speed averaged over a calendar month by

$$\overline{u}_{month} = (1/N_{month}) \sum_{t \in month} u(t) \qquad (1)$$

Table 1. Data From IABP Data Set That Are Used in This Study[a]

Year	Number of Buoys	Number of Tracks		Total Number of Speed Values	Seasonal Number of Speed Values	
		Winter	Summer		Winter	Summer
1979	11	10	10	12,595	5876	6719
1980	24	23	15	15,346	6403	8943
1981	24	16	18	13,736	5147	8589
1982	19	15	12	13,846	7256	6590
1983	17	12	9	9146	4926	4220
1984	11	6	8	9962	6994	2968
1985	17	10	15	12,056	6835	5221
1986	25	18	19	23,885	13,648	10,237
1987	34	18	29	28,141	15,570	12,571
1988	35	23	29	27,659	13,018	14,641
1989	22	21	10	15,398	10,320	5078
1990	19	18	16	13,673	7988	5685
1991	32	24	26	27,060	15,404	11,656
1992	37	32	27	31,283	16,140	15,143
1993	35	27	25	30,791	20,996	9795
1994	21	16	13	21,748	15,477	6271
1995	10	10	2	9461	9092	369
1996	11	11	9	15,769	11,040	4729
1997	10	10	6	10,756	7115	3641
1998	14	13	6	13,725	11,409	2316
1999	8	7	5	5936	3378	2558
2000	12	11	7	7664	4851	2813
2001	35	28	31	34,030	21,224	12,806
2002	49	46	35	14,074	10,308	3766
2003	54	39	38	9315	5651	3664
2004	52	40	37	10,771	6347	4424
2005	50	35	35	7422	4078	3344
2006	53	30	47	10,303	5821	4482
2007	114	83	101	24,240	12,468	11,772

[a]For each year, the number of buoys, buoys' tracks for each season, and corresponding speed values used in the present study are indicated. Winter and summer periods are from 1 December to 15 May and from 15 June to 30 September, respectively.

where N_{month} is the number of 12 hourly speed values for the month under study. It ranges from 116 to 5432. We chose this monthly timescale because it is short enough to document intraannual variations, as well as long enough to contain enough speed values for a statistically significant estimate of the mean. Because there exist time and spatial correlations in the velocity field [*Thorndike*, 1986; P. Rampal et al., Arctic sea ice velocity field: General circulation and turbulent-like fluctuations, submitted to *Journal of Geophysical Research*, 2008], the uncertainty on the estimate of the monthly speed $\overline{u}$ cannot be obtained directly from the central limit theorem and the number N_{month} of samples in the distribution, as those N_{month} samples are not independent of each other. Instead, we estimate these errors using a bootstrap method. In order to empirically find how the error $\Delta\overline{u}/\overline{u}$ depends on N_{month}, we consider separately each month and we randomly picked q times ($q \geq 10$) n speed values (n ranging from 5 to 150) for this month, taking care not to pick the same value twice, with the condition that $q \times n \approx 0.75 N_{month}$ (i.e., we overall pick about 75% of the set). For a given n, we therefore obtain q distributions of speed values for which we calculate their means. The standard deviation $\Delta\overline{u}$ on the $\overline{u}$ values is then computed. Figure 3a displays the results for a particular month, i.e., September 1987. Doing so for all the months between January 1979 and December 2007, we obtain that $\Delta\overline{u}$ decreases with n as follows:

$$\Delta\bar{u}_{bootstrap} = \frac{A\bar{u}_{bootstrap}}{n^{\lambda}} \qquad (2)$$

where $\overline{u}_{bootstrap}$ is the value of the mean found for a particular distribution (see Figure 3b). The exponent λ is approximately equal to 0.3, and A is equal to 0.6. In our analysis we use relation (2), replacing n by N_{month}, to estimate the uncertainty of $\overline{u}$. We note that relation (2) differs from the error estimate given by the central limit theorem for which $A = 1$ and $\lambda = 0.5$: the actual error is thus larger than the one given by the central limit theorem (as long as $n \geq 13$, as expected in the presence of correlations.

[7] Figure 4a shows the monthly mean speed between January 1979 and December 2007 for the Central Arctic data set. Figure 4a also shows the 12-month running mean. A linear fit to the data (in the least squares sense, weighted by the error bars) gives an increasing trend with a slope of 5.6 ($\pm$1.1) $\times$ 10^{-2} km d^{-1} a^{-1}. The error on the slope is estimated by a chi-2 test. A Fourier transform of the detrended signal reveals a peak at the 12-month period and thus a strong annual cycle (see Figure 4b). To further describe the annual cycle, we computed the mean speed for each calendar month, by averaging over the period 1979–2007 the mean speed values of the detrended signal that correspond to a given calendar month (see Figure 4c). A sinusoidal fit to the data (in the least square sense, weighted by the error bars) gives a maximum around September and a minimum around March. As expected by the Fourier transform of the monthly mean speed signal, the amplitude of this sinusoidal function is about 1.5 km d^{-1}, and its period is about 12 months. Thus, this strong seasonal variability is out of phase, lagging by about 6 months, with respect to the sea ice extent seasonal variability. We also estimated the trend over the period 1979–2007 for each

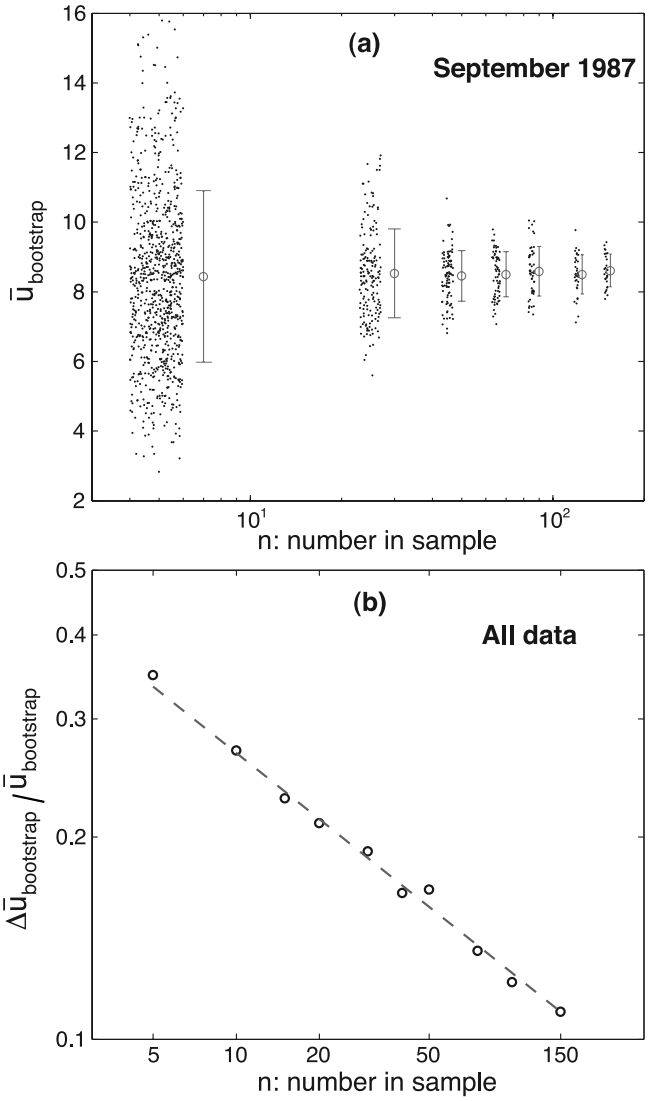

Figure 3. (a) Estimation of the monthly mean speed uncertainty using a bootstrap method for the month of September 1987. A number q of random sets of n values are picked, and theirs associated means $\overline{u}_{bootstrap}$ are computed (black dots). For clarity, we drew each dot at abscise x defined as $x = n + \rho$ where ρ is a random value between -2 and 2. The dispersion $\Delta\overline{u}_{bootstrap}$ (standard deviation) of the q means $\overline{u}_{bootstrap}$ is computed and shown as vertical bars. (b) Dependence of $\Delta\overline{u}_{bootstrap}/\overline{u}_{bootstrap}$ on the number of samples n. A general trend $\Delta\overline{u}_{bootstrap} = A \times \overline{u}_{bootstrap} n^{-\lambda}$ is obtained, with $A = 0.6$ and $\lambda = 0.3$.

calendar month and we find that all are positive excepting for February which shows a small and insignificant negative trend ($-2.0 \pm 5.0 \times 10^{-2}$ km d^{-1} a^{-1}). The maximum trends are observed in late summer–early winter and particularly for September with $9.0 \pm 4.0 \times 10^{-2}$ km d^{-1} a^{-1}. We conclude that the seasonal variability of the mean speed of sea ice increased over the last 29 years.

3.2. Seasonal Averages of Buoy Speeds

[8] We calculate the mean speed for winter and summer seasons separately (Figure 5). Winter and summer means are computed between 1 December and 15 May of the following year, and between 15 June and 30 September, respectively. The error bars are computed using equation (2), which is likely to overestimate the uncertainty at the seasonal scale. Linear fits computed by least squares using the errors as weights give significant positive trends of 6.4 ($\pm$1.7) $\times 10^{-2}$ km d^{-1} a^{-1} (i.e., 17% ($\pm$5.7%) increase per decade) for winter and 5.1 ($\pm$1.2) $\times 10^{-2}$ km d^{-1} a^{-1} (i.e., 8.5% ($\pm$2%) increase per decade) for summer.

4. Are the Mean IABP Buoy Speeds Representative of the Mean Arctic Sea Ice Speeds?

[9] So far, we have analyzed the IABP buoy speeds, showing there exists a significant increase of the monthly and seasonal means over the last 29 years. The question arises as to whether this increase is a direct signature of a similar increase of the overall Arctic sea ice speed, i.e., averaged over the whole sea ice extent. This leads us to examine spatial and temporal sampling issues, since the IABP buoy trajectories do not evenly sample the Arctic.

[10] We formulate the following null hypothesis: The Arctic sea ice motion is characterized by a monthly averaged speed that is annually constant. In other words, the monthly averaged speed for a given calendar month, e.g., January 2000, is drawn from a distribution that is the same for all the months of January between 1979 and 2007. We thus allow for a seasonal, i.e., intraannual, variability, but hypothesizes that there is no interannual changes (12-month periodic stationary). The question is then to check whether the observed increase of buoy speeds over the 29 years (see section 3) could be due solely to a change in spatial sampling from one year to the next, i.e., do IABP buoys tend to sample fast-moving regions more often in the later years compared to early years. To address this, we will construct a mean speed field over the whole Arctic for each month (hence 12 velocity fields) (see section 4.1). Then, we estimate what would have been the buoy monthly mean speeds, as sampled by the actual IABP trajectories, if the underlying speed fields were indeed stationary and we conclude (see section 4.2).

4.1. Constructing the Mean Speed Fields

[11] For each of the 12 months, January–December, we generate a mean speed field from the IABP data set, say that we do not consider the mean drifting directions. Namely, we compute the 12-h interpolated speed $\overline{u}$ at all positions $\mathbf{x}_N$ reached by buoys and for any given month as:

$$\overline{u}(\mathbf{x}_N) = \frac{1}{\sum_i w_i(\mathbf{x}_i)} \sum_i w_i(\mathbf{x}_i) u_i(\mathbf{x}_i) \tag{3}$$

where the summation is performed over all the buoy positions $\mathbf{x}_i$ selected in the following way: the positions $\mathbf{x}_i$ are recorded during the same given month (e.g., all the buoys positions recorded for all the 29 months of January), and contained in the disk centered on $\mathbf{x}_N$ with a radius of $L =$ 200 km (if the given month is a winter's month) or $L =$ 100 km (if it is a summer's month) (Rampal et al., submitted manuscript, 2008). We define the weight $w_i(\mathbf{x}_i)$ as:

$$w_i(\mathbf{x}_i) = e^{-r^2/2l^2} f(r) \tag{4}$$

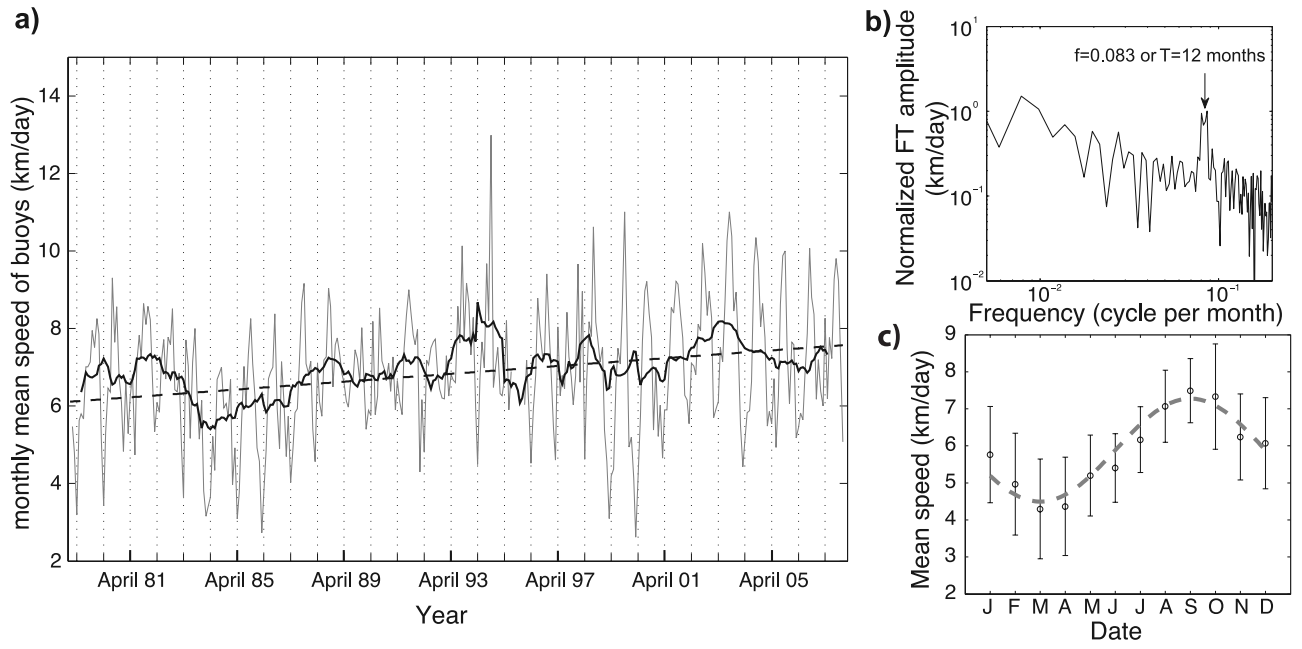

Figure 4. (a) Monthly mean speed for IABP buoys from January 1979 to December 2007. The monthly means are computed from the 12 hourly speeds data set and plotted as the light gray line. The 12-month running mean is plotted as the bold dark line. The least squared fit (weighted by the uncertainty) of the data is plotted as the dashed dark line and gives a slope of 5.6 (±1.1) × 10^{-2} km d^{-1} a^{-1}. The error on the slope is estimated from a chi-2 test. (b) The normalized amplitude of the Fourier Transform of the monthly signal is also plotted and shows a peak at T = 12 months. (c) The averaged annual cycle in the mean speed of sea ice reveals an absolute amplitude of about 1.5 km d^{-1} (in agreement with the amplitude of the peak in the FT) with a maximum occurring around September and a minimum occurring around March. The error bars are the standard deviation of the monthly values.

where $r = \|\mathbf{x}_N - \mathbf{x}_i\|$, l is the smoothing length defined as $l = L$, and $f(r)$ is a correction term that accounts for the spatial heterogeneity of buoys positions. Ideally, the sample positions $\mathbf{x}_i$ would evenly cover the L-radius disk; this is unfortunately not the case, as they follow buoy trajectories. Instead of following a $N(<r) \sim r^2$ law, the actual number of pairs of distances $\|\mathbf{x}_i - \mathbf{x}_j\| < r$ grows initially slower with r, and therefore do not evenly sample the disk. Not correcting for this effect would imply having effective smoothing lengths varying with $\mathbf{x}$, that would generally be less than l. We therefore homogenize the smoothing by introducing the correction $f(r) = r^2/N(\|\mathbf{x}_N - \mathbf{x}\|_i < r)$. Note that $f(r)$ is defined up to a multiplicative constant, which disappears with the normalization in equation (3).

[12] To illustrate this correction, we show on Figure 6a an example of the spatial heterogeneity of the velocity measurements around the position of buoy 66739 on 13 January 2007, by plotting all the 4630 buoy positions within 400 km for all the months of January between 1979 and 2007. This is compared to an equivalent of 4630 positions synthetically computed following a Poissonian repartition in Figure 6b. Figure 6c displays the corresponding number $N(\|\mathbf{x}_N - \mathbf{x}_i\| < r)$ of observations as a function of r, for Figures 6a and 6b, showing clearly the effect of the spatial heterogeneity of the data. Also, to give a more quantitative view of this correction, we computed its relative weight (in %) in each computed means. The distribution of these relative weights has a mean of 2%, a standard deviation of 4% and a maximum of 53%. These statistics argue for the need to take into account of the correction induced by $f(r)$ in the computation of the means.

4.2. Monthly Mean Speeds Estimated From the Interpolated Speed Fields

[13] Using the interpolated speed fields, we compute the monthly means $\overline{u}_\emptyset$ obtained when sampling these fields with the actual IABP buoy positions of that month. Figure 7 shows the monthly mean speed time series obtained under our null hypothesis, compared to the actual monthly means of Figure 4. The annual cycle is still present in the signal. On the other hand, a linear fit to the data (in the least squares sense) weighted by errors as computed following equation (2), gives a quasi-null trend of 6.8 (±3.2) × 10^{-5} km d^{-1} a^{-1}, i.e., only 0.1% of the actual trend directly estimated from the IABP buoy speeds.

[14] Similarly, the seasonal mean speed signals computed under our null hypothesis give trends of 6.6 (±3.1) × 10^{-5} and 6.9 (±2.7) × 10^{-5} km d^{-1} a^{-1}, for winter and summer, respectively, i.e., 0.1% and 0.14% of the actual trends estimated from the IABP buoy's speeds.

[15] We therefore conclude that the bias introduced by the spatial sampling of the buoys trajectories cannot explain the observed increase of buoy speeds over the 29 years, and consequently that the observed acceleration of buoy motion

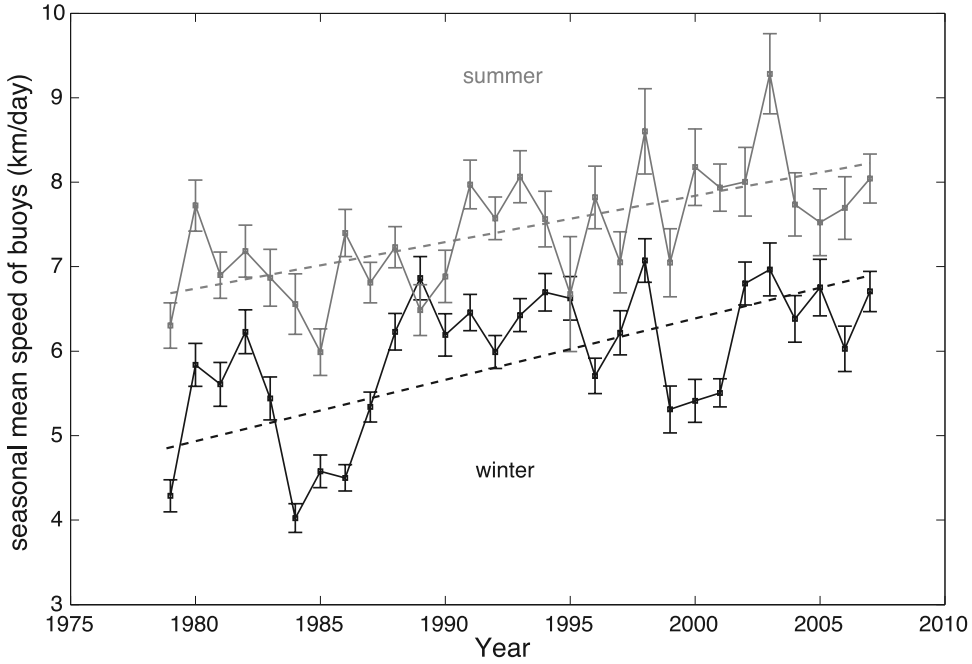

Figure 5. Buoy mean speed for the winters and summers of 1979–2007. Winter means are plotted in black, and summer means are plotted in gray. The error bars are estimated following equation (1). The weighted linear fits of the data are plotted as dashed lines for winter and summer. The trends are 6.4 (±1.7) × 10^{-2} km d^{-1} a^{-1} (i.e., 17% increase per decade) for winter and 5.1 (±1.2) × 10^{-2} km d^{-1} a^{-1} (i.e., 8.5% increase per decade) for summer.

is significant and representative of an overall acceleration of the sea ice motion over the Arctic basin.

5. Increase of the Mean Deformation Rate of the Sea Ice Cover Over the Last 29 Years

[16] Excepting the Fram Strait and the Barents Sea, one can consider the Arctic sea ice cover as moving in a confined basin, with velocities vanishing to zero as one get closer to the coasts. Consequently, given the strong increase of the sea ice mean speed during the last three decades, we expect an acceleration of sea ice mean deformation rate (see section 4.1). As a first-order approximation, we consider that the relative increase of sea ice speed is the same everywhere in the Arctic basin. Then, considering (1) sea ice drifting speed $u = 0$ at the coasts and maximum in the center of the basin, i.e., at about $L = 1000$ km from the coasts, and (2) that velocity gradients and strain rate tensor are linearly linked as $\dot{\varepsilon} = (\nabla\mathbf{u} + \nabla\mathbf{u}^T)/2$, i.e., the norm of the strain rate tensor $\dot{\varepsilon}$ equals $\|\nabla\mathbf{u}\|$, one can estimate the averaged rate of increase of the strain rate as follows:

$$\frac{\overline{\Delta \,\|\, \dot{\varepsilon} \,\|}}{\Delta t} = \frac{\overline{\Delta \,\|\, \nabla\mathbf{u} \,\|}}{\Delta t} = \frac{1}{L}\frac{\overline{\Delta u}}{\Delta t} \tag{5}$$

[17] Using equation (5) and the rates of increase of sea ice drifting speed determined in section 3 (6.4 × 10^{-2} km d^{-1} a^{-1} for winter and 5.1 × 10^{-2} km d^{-1} a^{-1} for summer), we obtain that the deformation rates would have increased by 6.4 × 10^{-5} d^{-1} a^{-1} for winter and 5.1 × 10^{-5} d^{-1} a^{-1} for summer.

[18] In what follows, we check (1) whether the positive trends in sea ice drifting speed found for winter and summer indeed imply positive trends in sea ice deformation rate for both seasons and (2) to what extent our first-order estimates of these trends are correct. To do so, we estimate the sea ice strain rate for the period 1979–2007 from the dispersion of pairs of buoys. We present in section 5.1 a methodology that allows relating dispersion and deformation. The results of our analysis are given in section 5.2, and discussed in section 6.

5.1. Relation Between Dispersion of Buoys and Sea Ice Deformation

[19] The dispersion of pairs of buoys can be directly linked to sea ice cover deformation [*Rampal et al.*, 2008] using an approach based on the methodology developed by Richardson for turbulent flows [*Richardson and Stommel*, 1949; *Martin and Thorndike*, 1985]. We study how the dispersion of pairs of buoys depends on both (1) their initial separation L and (2) the time τ during which they disperse. In Figure 8, two buoys numbered 1 and 2 with absolute positions $\mathbf{x}_1$ and $\mathbf{x}_2$, respectively, and with separation $\mathbf{y} = \mathbf{x}_2 - \mathbf{x}_1$, are considered. If these two buoys initially separated by $L = \|\mathbf{y}(0)\|$ are observed after a time τ, a change in separation is observed. Our notations are: $\mathbf{y}(0)$ has magnitude L and $\mathbf{y}(\tau)$ has magnitude $l(\tau)$. We define the change in separation Δr as $\Delta r(\tau) = \|\mathbf{y}(\tau)\| - \|\mathbf{y}(0)\| = l(\tau) - L$.

[20] In fluid mechanics, the dispersion process is characterized by the mean square change in separation $\langle \Delta r^2 \rangle$. From a solid mechanics perspective, it appears more pertinent to consider the rate $D = \Delta r / L\tau$ instead of the change in separation Δr. $\dot{D}$ is analogous to a deformation rate,

measured in d^{-1}. Neither Δr nor $\dot{D}$ are sensitive to solid rotations. They only quantify the deformation due to divergence, convergence, and/or shear. However, this methodology does not allow distinguishing divergence/convergence from shear, as at least triplets of buoys should be used to compute the full strain tensor. When analyzing the whole Arctic basin, we again made a distinction between winter (from the beginning of December to mid-May) and summer (from mid-June to the end of September). Separately for both seasons, and for each year of the period, we computed the distributions of $\dot{D}$. *Rampal et al.* [2008] studied how $\dot{D}$ depends on the scales L and τ. In order to examine how the deformation changed in 29 years, and to minimize sampling issues due to this scale dependence, we considered the statistics of $\dot{D}$ for L between 50 and 500 km and τ between 3 h and 1 day, hence only a decade in scale range. For each year, the associated distributions for winter and summer are characterized by their standard deviation $\sigma_{\dot{D}}$. In this way, we measure how a cluster of passive tracers of initial size L typically disperses after a time τ or, in other words, how the associated region containing these tracers deforms. The choice of the standard deviation of $\dot{D}$ rather than its mean is partly motivated by the fact that in the limit of small deformation rates (i.e., for large timescales and spatial scales), only the standard deviation characterizes the deformation process. In the work of *Rampal et al.* [2008], we showed that σ_D, i.e., the standard deviation of $D = \Delta r/L$, is correlated to the total deformation ε_{tot}. For two particular cases, define SHEBA and SIMI experiments, we calculated the strain tensor and the total deformation ε_{tot} from multiplets of buoys. We found that our strain proxy σ_D is proportional to ε_{tot} with a factor of about 2 and a correlation of $R = 0.8$. We concluded that the total strain rate $\sigma_{\dot{D}}$ can be viewed as a good proxy of the total deformation rate $\dot{\varepsilon}_{tot}$.

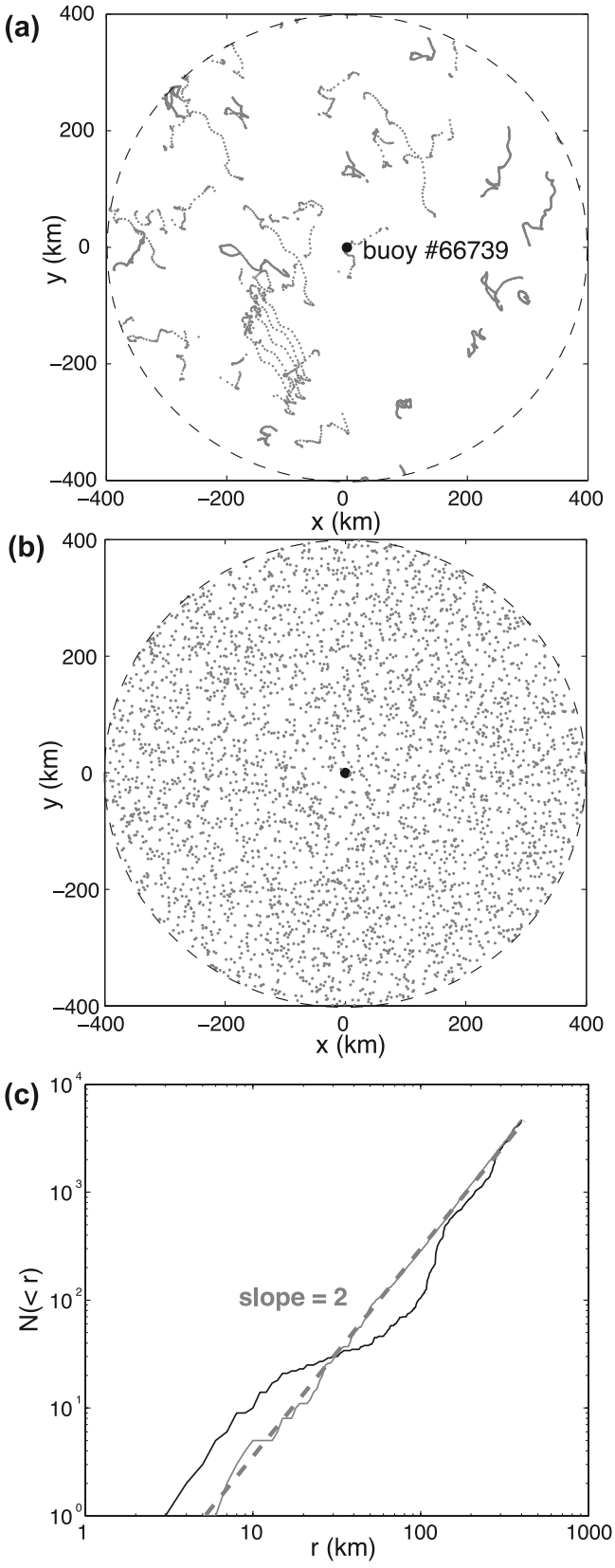

Figure 6. Illustration of the spatial heterogeneity of the buoy positions available during any calendar month of January between 1979 and 2007. Here the position of the buoy 66739 recorded on 13 January 2007 is set as the reference position. (a) The 4630 buoy positions found in the January months of 1979–2007 plotted within 400 km of the reference position. This can be compared to (b) a set of 4630 synthetic positions computed following a Poisson distribution. (c) Number $N(<r)$ of positions contained in the disk of radius r centered on (0,0) for actual buoy positions (dark line) and synthetic positions (gray line). $N(<r)$ follows a r^2 law (gray dashed line) for the Poisson distribution. For IABP buoys, $N(<r)$ deviates from this law. The term $f(r)$ in equation (4) is introduced to correct for this effect.

5.2. Results

[21] Figure 9 shows that, despite large uncertainties on the estimates (see Appendix A for details on uncertainty estimation), the strain rate increases significantly over the 29 years, at a rate of 2.4 (±0.4) × 10^{-4} d^{-1} a^{-1} (i.e., 51% ±8.5% increase per decade) for winter and 2.6 (±0.6) × 10^{-4} d^{-1} a^{-1} (i.e., 52% ±12% increase per decade) for summer. The trends obtained from our analysis are one order of magnitude greater than the first-order estimates previously obtained with the hypothesis of an homogeneous increase of sea ice speed (in %) over the Arctic basin, and so of an homogeneous increase of the deformation rate. As sea ice strain rate is highly heterogeneous [*Marsan et al.*, 2004; *Rampal et al.*, 2008], this first-order approximation strongly underestimates the rates of increase of sea ice deformation

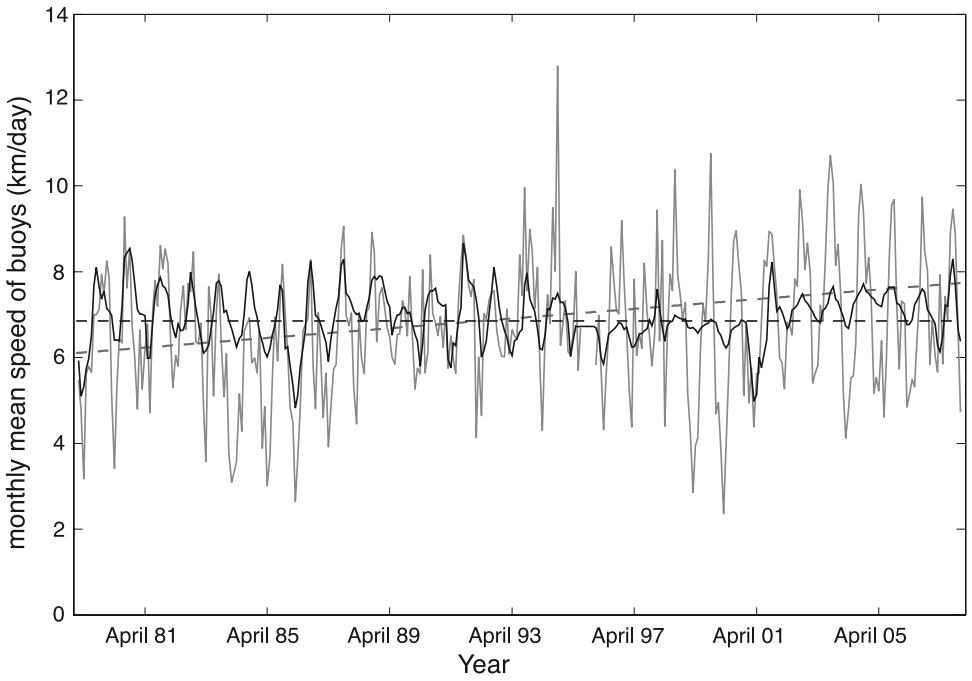

Figure 7. Monthly mean speed time series $\overline{u}(t)$ (gray line) and $\overline{u}_{\emptyset}(t)$ (black line), obtained for the actual IABP buoys and for the IABP buoys under our null hypothesis, respectively. The dark dashed line is the linear fit of $\overline{u}_{\emptyset}(t)$ (weighted by the error bars). This later gives a quasi-null trend of 6.8 ($\pm$3.2) $\times$ 10^{-5} km d^{-1} a^{-1}, i.e., only 0.1% of the actual trend computed for $\overline{u}(t)$ (dashed gray line).

rates. Furthermore, as shear dominates the total strain rate within the Arctic basin [*Stern and Moritz*, 2002], these trends also suggests that shear deformation, and therefore the associated Coulombic faulting [*Schulson*, 2004; *Weiss et al.*, 2007], significantly increased during the last 29 years.

6. Discussion

[22] We found that both Arctic sea ice speeds and deformation rates significantly increased over the past 29 years. Why did these increases occur? Two main hypotheses can be formulated.

[23] 1. The intensity of the external forcing increased, i.e., the oceanic currents and/or winds strengthened over the period.

[24] 2. These increases are the consequence of the thinning of the sea ice cover that implies a decreasing mechanical strength, hence an easier fracturing and deformation. This would in turn facilitate melting and export out of the Arctic basin, thus reinforcing the albedo feedback loop and possibly the polar amplification.

6.1. External Forcing

[25] Winds and, to a lesser extent ocean currents, are considered to be the two main forcing terms for sea ice drift and deformation. It is not possible to check from the sparse data available a hypothetic trend on ocean current velocity magnitudes over the whole Arctic basin for the period 1979–2007. On the other hand, for the atmosphere, the Arctic Oscillation (AO) index [*Thompson and Wallace*, 1998] furnishes an indication of the strength of the circulation over the Arctic: During anticyclonic (negative AO) circulation regimes, atmospheric pressure is higher, wind speed is lower, and supposedly sea ice is thicker and its extension greater [*Richter-Menge et al.*, 2006; *Rigor et al.*, 2002]. During positive AO phases, wind speed is greater, wind divergence produces more sea ice opening, and export of sea ice out of the basin is facilitated [*Richter-Menge et al.*, 2006; *Rigor et al.*, 2002]. Since 1979, the annually averaged AO index (provided on the Web by the National Weather Service of the NOAA at http://www.cpc.ncep.noaa.gov/products/) was particularly high from 1989 to 1994, but then fluctuated between negative and positive

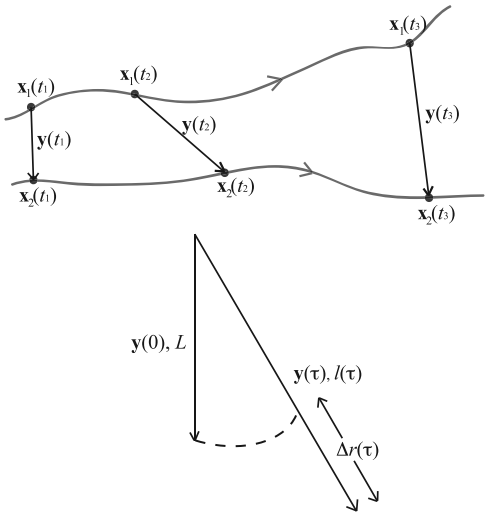

Figure 8. For a pair of buoys located at $\mathbf{x}_1$, $\mathbf{x}_2$ and separated by $\mathbf{y} = \mathbf{x}_2 - \mathbf{x}_1$, the change in separation at time τ is denoted $\Delta r(\tau) = \|\mathbf{y}(\tau)\| - \|\mathbf{y}(0)\|$.

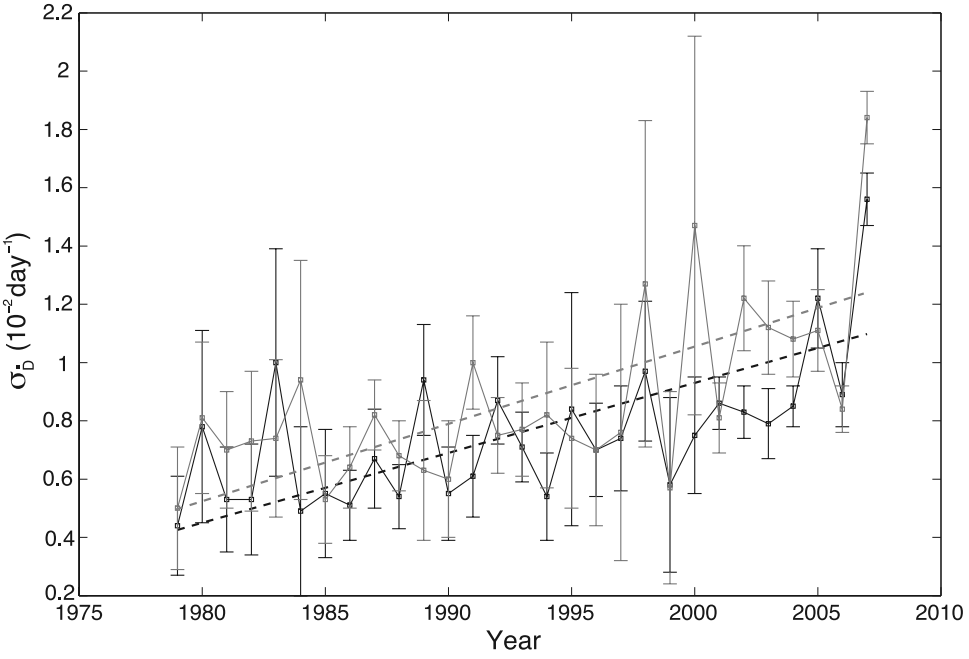

Figure 9. Sea ice mean strain rate proxy of the winters and summers of 1979–2007. This proxy is calculated for timescales shorter than 1 day and spatial scales ranging from 50 km to 500 km (see text). Winter mean series are drawn in black, while summer mean series are in gray. Associated error bars are estimated from a bootstrap method (see Appendix A). The weighted linear fits of the data are plotted as dashed lines and give trends of 2.4 (±0.4) $\times$ 10^{-4} d^{-1} a^{-1} (i.e., 51% ±8.5% increase per decade) for winter and 2.6 (±0.6) $\times$ 10^{-4} d^{-1} a^{-1} (i.e., 52% ± 12% increase per decade) for summer.

values, without positive trend. In addition, we did not observe any significant correlation between the seasonally averaged (winter and summer) AO index and our seasonally averaged sea ice mean speeds or deformation rates ($R^2 < 0.2$ in all cases). This suggests that the trends reported here are unlikely to be a consequence of a stronger wind forcing. To further test this point, we used the ERA-40 reanalysis data set provided by the ECMWF (http://data.ecmwf.int/data/d/era40_mnth/) that gives the two components $\overline{u}_x^{wind}$ and $\overline{u}_y^{wind}$ of the monthly mean wind velocity vector $\overline{\mathbf{u}}^{wind}$ at 10 m height above the surface on a regular grid of 2.5° by 2.5° and for the period 1979–1999. From this data set, we first computed the monthly mean wind speed at each grid points.

[26] At high latitude, a 2.5° by 2.5° grid do not cover the Arctic basin homogeneously as numerous grid points lie in the vicinity of the North Pole. Consequently, before computing a mean wind speed value for the Arctic basin, we interpolated the previous mean speeds on a regular grid of 200 km by 200 km using a linear method (i.e., linear weighting of the three nearest speed values). Finally, we computed the monthly mean wind speed $\overline{u}^{wind}(t)$ for the whole Arctic basin and for each month of 1979–2000 by averaging the speeds of the monthly mean field that lie in the central Arctic region (see Figure 1). Figure 10 displays $\overline{u}^{wind}(t)$ between January 1979 and December 1999. A linear fit (in the least square sense) of the data gives a trend of 1.2 (±0.8) $\times$ 10^{-3} m s^{-1} a^{-1}, i.e., an increase of 0.4% per decade. We thus conclude that there is no significant increase (in terms of wind speed) of the atmospheric forcing over the period 1979–2000. This does not rule out a possible role of atmospheric circulation patterns onto, e.g., sea ice export through Fram Strait [*Kwok and Rothrock*, 1999; *Kwok et al.*, 2004].

6.2. Sea Ice Deformation, Thinning, and Export

[27] Arctic sea ice thinning over the last decades is now clearly recognized: the annual mean ice draft determined from submarine sonars declined from about 3.4 m in 1980 to about 2.3 m in 2000, corresponding to an average decrease of 1.2 m in thickness [*Rothrock et al.*, 2008]. This decline most likely leads to a decrease of the sea ice mechanical strength, which then favors an increase of sea ice deformation rates and associated fracturing during the period. As a fragmented ice cover is easier to move, this may also leads to the increase of sea ice mean speed observed in the Central Arctic and could possibly facilitate sea ice export through Fram Strait. *Kwok and Rothrock* [1999] and *Kwok et al.* [2004] examined the sea ice area flux through Fram Strait from passive microwave ice motion data, and found a small positive trend over the period 1978–2002.

[28] Here, we consider the sea ice mean speed along the Greenland coast (see Figure 1). We note that the sea ice area flux estimated in the works cited above depends on both magnitude and direction of velocity vectors that crossed the Fram Strait line, whereas here we only consider a scalar. From the actual sea ice mean speed increase in the central Arctic, one could hypothesize that, over the period of interest, the sea ice mean speed along the Greenland coast also increased. A positive trend of 13 $\times$ 10^{-2} km d^{-1} a^{-1}

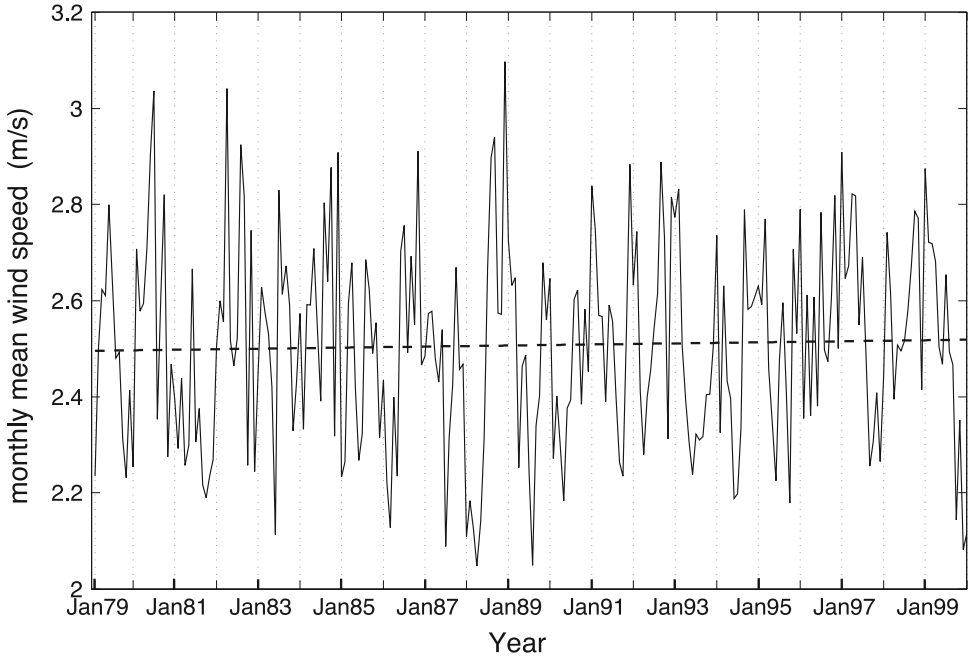

Figure 10. Monthly mean wind speed $\overline{u}^{wind}(t)$ between January 1979 and December 1999. The means are computed from the two velocity components of the estimated wind velocity vector of the ERA-40 reanalysis data set. A linear fit (in the least square sense) of the data gives a trend of 1.2 (±0.8) × 10^{-3} m s^{-1} a^{-1} (i.e., an increase of 0.4% per decade) and is drawn as a dashed black line.

was recently reported for the Fram Strait and the northern part of the Barents Sea for the period 1979–2005 from a combined analysis of satellite and buoy data [*Pavlov and Pavlova*, 2007], twice as large as our trends reported in section 3 for the central Arctic. As the buoy trajectories are too sparse south of Fram Strait, we analyzed the satellite-derived velocity estimates provided by the Polar Remote Sensing Group of the Jet Propulsion Laboratory (http://www-radar.jpl.nasa.gov/rgps/). The sea ice velocities are computed for winters between 1979 and 2004 with a sampling of 2 days and their uncertainties are about 10% [*Kwok and Rothrock*, 1999]. From this data set, we selected the velocities in a region along Greenland and below approximately 82°N of latitude (see Figure 1). For the period 1979–2004, we calculated the mean winter speeds, averaged over 5 1/2 months, i.e., between December and 15 May (Figure 11). A weighted linear fit of the data gives a positive trend of 5.6 (±2.0) × 10^{-2} km d^{-1} a^{-1} (i.e., 7% ±2.5% increase per decade). However, this trend is less significant than those observed for the Arctic basin, as the result of large uncertainties in mean drift estimates partly due to rather large uncertainties on the satellite-derived velocities. Nevertheless, we may interpret this positive trend as (1) a response to the change in the Arctic basin kinematics presented above, this later favored by a thinning of the sea ice cover in the central Arctic, and/or (2) as a direct effect of thinner ice on sea ice kinematics in the region south of Fram Strait.

[29] Although a significant correlation ($R^2 \approx 0.4$) was found between the sea ice area flux through Fram Strait and the NAO index from 1978 to 2002 [*Kwok et al.*, 2004], we did not find here any significant correlation ($R^2 < 0.1$) between the winter's AO index and our winter mean speed in the region southward to the Fram Strait.

[30] If sea ice fracturing and deformation are facilitated by thinning, the reverse might be true, as a more fractured/fragmented sea ice cover means (1) more lead opening, stronger melting during summer, and a delayed refreezing in early winter and (2) possibly easier export of ice out of the Arctic basin. Note, however, that more fracturing would imply an increase of ice production later in winter, a negative feedback that could partially compensate for this effect, although young, thin ice is more prone to fracture again. This coupling between sea ice deformation and fracturing in one hand, and sea ice extent and thickness on the other hand can easily explain how the sea ice drift annual cycle is out of phase, lagging by 6 months, with the sea ice extent annual cycle [*Comiso et al.*, 2008] as well as with the sea ice thickness annual cycle recently quantified by *Rothrock et al.* [2008]. Consequently, sea ice kinematics and fracturing could strengthen the albedo feedback loop, polar amplification and the associated decline of the Arctic sea ice cover. Classical sea ice models, based on a continuum mechanics, fluid-like framework with a viscous-plastic or an elastic-viscous-plastic rheology, are not able, by nature, to correctly represent the brittle fracturing/faulting of sea ice [*Coon et al.*, 2007; *Rampal et al.*, 2008; *Schulson*, 2004; *Weiss et al.*, 2007], as well as the induced strain rate fields [*Thomas*, 1999; L. Girard et al., Evaluation of two high-resolution sea ice models on the basis of statistical and scaling properties of Arctic sea ice drift and deformation, submitted to *Journal of Geophysical Research*, 2008]. One can therefore wonder about their ability to properly model the role of fracturing/faulting into the albedo feedback loop.

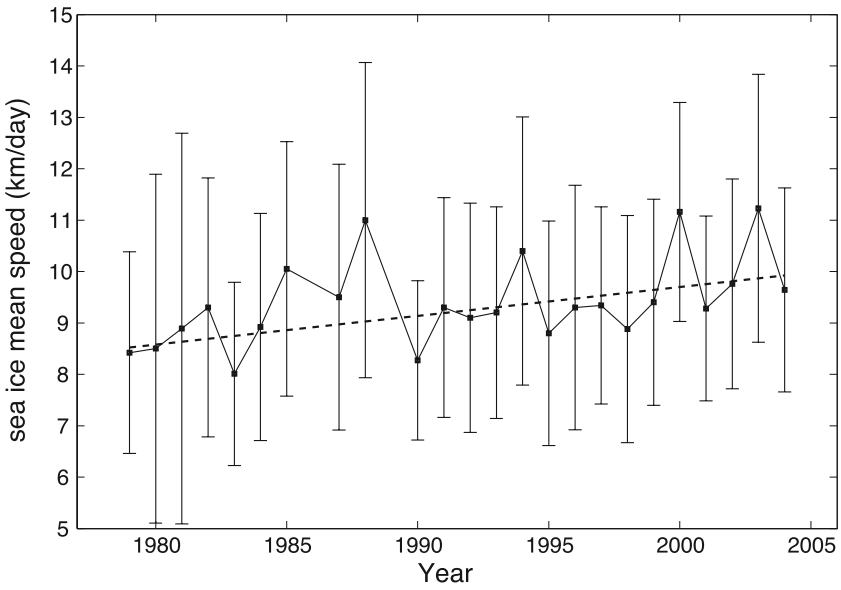

Figure 11. Sea ice mean drift along the Greenland coast during winter from 1979 to 2004. The means are computed from a Special Sensor Microwave/Imager–derived velocity data set and averaged from 1 December and 15 May. The error bars are estimated from the bootstrap method presented in section 3. A weighted linear fit is shown (dashed line) and gives a trend of 5.6 (±2.0) $\times 10^{-2}$ km d^{-1} a^{-1} (i.e., 7.5% increase per decade).

This might explain partly why climate models underestimate sea ice decline [*Stroeve et al.*, 2007; *Serreze et al.*, 2007].

6.3. Year 2007

[31] The year 2007 might be a good illustration of the positive feedback between deformation and sea ice decline.

[32] Exceptionally large mean deformation rates are recorded both in winter and summer 2007 (see Figure 9). Moreover, their associated error bars are small, as the result of the large number of buoys available during this year. The 2007 deformation rate value for winter equals 6 standard deviations of the linear fit error from the fit for the winters 1979 to 2006. For summer, this is about 3.5. This illustrates well that these 2007 values are indeed exceptionally large compared to the 29-year linear trends, just as the 2007 September sea ice extent was exceptional compared to the 29-year average decline of sea ice minimum extent [*Stroeve et al.*, 2008].

[33] Why do the records of 2007 deviate so strongly from the 1979–2006 positive trend, and is this related somehow to the 2007 sea ice minimum extent? The role of the mechanical behavior of sea ice and its deformation on the ice-albedo feedback loop, and thus on sea ice thinning, is induced by the fracturing/faulting of the cover, which result from its elasto-brittle rheology [*Weiss et al.*, 2007; *Rampal et al.*, 2008]. Brittle behavior is by nature a highly nonlinear, threshold mechanism. The exceptional 2007 deformation rates may suggest that the mean sea ice thickness, and so its mechanical strength, has passed a threshold over a large part of the Arctic below which its fracturing and collapse is highly facilitated, leading to an abrupt change in its mechanical response to the winds and currents.

[34] *Perovich et al.* [2008] showed that the solar heating of the upper ocean was the primary source of heat that led to an extreme sea ice melting during the summer 2007 in the Beaufort Sea region. They argued for an increase in area of open water as the cause of the upper ocean heating and asked for the process that triggered this increase. A stronger fracturing, favored by the thinning of sea ice, is a possible cause of such increase in area of open water. This is in agreement with *Lindsay et al.* [2008] who recently concluded that the unusual retreat of the sea ice in 2007 was preconditioned by decades of gradually warming temperatures and the replacement of older ice by younger ice, resulting in a thinner ice pack. This preconditioning may have lead the 2007 sea ice cover to pass a threshold in mechanical strength, which would have in turn implied a strong melting/thinning of sea ice in some regions of the Arctic during summer 2007 [*Perovich et al.*, 2008], and facilitated its advection from the Pacific sector to the Atlantic sector of the Arctic basin in response to the persistent southerly winds recorded in summer 2007 [*Lindsay et al.*, 2008], and then finally participated to the 2007 sea ice shrinking.

7. Conclusions

[35] From an analysis of the IABP buoy trajectories data set from 1979 to 2007, we have shown the following:

[36] 1. The sea ice mean speed has substantially increased over the period (+17% per decade for winter and +8.5% for summer). A strong seasonal dependence of the mean speed is also revealed, with a maximum in October and a minimum in April.

[37] 2. The sea ice mean strain rate also increased significantly over the period (+51% per decade for winter and +52% for summer).

[38] 3. These increases in both sea ice mean speed and deformation rate are unlikely to be a consequence of a stronger atmospheric forcing, suggesting instead that sea ice

kinematics play a fundamental role in the albedo feedback loop and sea ice decline.

[39] 4. The September minimum sea ice extent of 2007 might be a good illustration of this interplay between sea ice deformation and sea ice shrinking, as we found that exceptionally large deformation rates affected the Arctic sea ice cover during all this year.

Appendix A: Estimating Uncertainties on $\sigma_{\dot{D}}$, the Standard Deviation of $\dot{D}$

[40] Time correlations (memory effects) are present in ice velocity records [*Thorndike*, 1986; Rampal et al., submitted manuscript, 2008], and can also be found in time series of ice deformation rates as approximated by the dispersion of pairs of buoys. An autocorrelation analysis reveals a correlation time of about 10 h for an initial separation of $L = 300$ km [*Rampal et al.*, 2008]. This correlation time becomes smaller for small L. In addition, strong spatial correlations are present in the deformation field [*Marsan et al.*, 2004]. Consequently, the errors on the estimation of $\sigma_{\dot{D}}$ cannot be obtained directly from the central limit theorem and the number N of samples. Instead, we estimate these errors from the same bootstrap method used in section 3.1, with the difference that the number of pairs of buoys N_p taken into account in each distribution, rather than the number of samples N, should be used as the number of independent variables. In each "annual" distribution, we randomly picked q times ($q \geq 10$), all the $\dot{D}$ values coming from n independent pairs of buoys, taking care not to pick the same pair twice, with the condition $q \times n \approx 0.75 N_p$. Then, we obtain q distributions of $\dot{D}$ values for which we calculate their standard deviation ${\sigma_{\dot{D}}}^{bootstrap}$. The dispersion of the ${\sigma_{\dot{D}}}^{bootstrap}$ values, i.e., their standard deviation noted $\delta{\sigma_{\dot{D}}}^{bootstrap}$, is computed for each given n. Finally, we obtain that $\delta{\sigma_{\dot{D}}}^{bootstrap}$ decreases with n as $\delta{\sigma_{\dot{D}}}^{bootstrap} = (A \times {\sigma_{\dot{D}}}^{bootstrap})/n^{\lambda}$ where A is about 0.9, and λ is approximately equal to 0.4. We note that this expression is similar to the error estimate given by the central limit theorem, with the important difference that the number of pairs of buoys N_p is considered instead of the number of samples N. Also, the values of A and λ differ slightly from $A = 1$ and $\lambda = 0.5$ as would be expected if the central limit theorem would apply.

[41] **Acknowledgments.** We thank I. Rigor from the Polar Science Centre of Seattle for the compilation and the distribution on the Web of the IABP data set. We also thank the ECMWF and the JPL for the compilation and the distribution of the ERA-40 data set and the SSM/I data set, respectively. Thanks also to the National Weather Service of the NOAA for the distribution of the AO index time series. A special thanks to the DAMOCLES European program and the Tara expedition who motivated this analysis (http://www.taraexpeditions.org). We thank an anonymous reviewer for his interesting and constructive remarks.

References

Alam, A., and J. A. Curry (1997), Determination of surface turbulent fluxes over leads in Arctic sea ice, *J. Geophys. Res.*, *102*, 3331–3343, doi:10.1029/96JC03606.

Colony, R., and A. S. Thorndike (1984), An estimate of the mean field of Arctic sea ice motion, *J. Geophys. Res.*, *89*, 10,623–10,629, doi:10.1029/JC089iC06p10623.

Comiso, J. C., C. L. Parkinson, R. Gersten, and L. Stock (2008), Accelerated decline in the Arctic sea ice cover, *Geophys. Res. Lett.*, *35*, L01703, doi:10.1029/2007GL031972.

Coon, M., R. Kwok, G. Levy, M. Pruis, H. Schreyer, and D. Sulsky (2007), Arctic Ice Dynamics Joint Experiment (AIDJEX) assumptions revised and found inadequate, *J. Geophys. Res.*, *112*, C11S90, doi:10.1029/2005JC003393.

Gascard, J. C., et al. (2008), Exploring Arctic transpolar drift during dramatic sea ice retreat, *Eos Trans. AGU*, *89*(3), doi:10.1029/2008EO030001.

Kwok, R. (2006), Contrasts in sea ice deformation and production in the Arctic seasonal and perennial ice zones, *J. Geophys. Res.*, *111*, C11S22, doi:10.1029/2005JC003246.

Kwok, R., and D. A. Rothrock (1999), Variability of Fram Strait ice flux and North Atlantic Oscillation, *J. Geophys. Res.*, *104*, 5177–5189, doi:10.1029/1998JC900103.

Kwok, R., G. F. Cunningham, and S. S. Pang (2004), Fram Strait sea ice outflow, *J. Geophys. Res.*, *109*, C01009, doi:10.1029/2003JC001785.

Lemke, P., et al. (2006), Observations: Changes in snow, ice and frozen ground, in *Climate Change 2007: The Physical Science Basis: Contribution of Working Group I to the Fourth Assessment Report of the Intergovernmental Panel on Climate Change*, pp. 350–355, Cambridge Univ. Press, New York.

Lindsay, R., and J. Zhang (2005), The thinning of Arctic sea ice, 1988–2003: Have we passed a tipping point?, *J. Clim.*, *18*, 4879–4894, doi:10.1175/JCLI3587.1.

Lindsay, R., J. Zhang, A. Schweiger, M. Steele, and H. Stren (2008), Arctic sea ice retreat in 2007 follows thinning trend, *J. Clim.*, *22*, 165–176, doi:10.1175/2008JCLI2521.

Lüpkes, C., T. Vihma, G. Birnbaum, and U. Wacker (2008), The influence of leads in sea ice on the temperature of the atmospheric boundary layer during polar night, *Geophys. Res. Lett.*, *35*, L03805, doi:10.1029/2007GL032461.

Marsan, D., J. Weiss, R. Lindsay, and H. Stern (2004), Scale dependence and localization of the deformation of Arctic sea ice, *Phys. Rev. Lett.*, *93*, 17, doi:10.1103/PhysRevLett.93.178501.

Martin, S., and A. S. Thorndike (1985), Dispersion of sea ice in the Bering Sea, *J. Geophys. Res.*, *90*, 7223–7226, doi:10.1029/JC090iC04p07223.

Maykut, G. A. (1982), Large-scale heat exchange and ice production in the central Arctic, *J. Geophys. Res.*, *87*, 7971–7984, doi:10.1029/JC087iC10p07971.

Moritz, R. E., C. M. Bitz, and E. J. Steig (2002), Dynamics of recent climate change in the Arctic, *Science*, *297*, 1497–1502, doi:10.1126/science.1076522.

Pavlov, V. K., and O. A. Pavlova (2007), Increasing sea ice drift velocities in the Arctic Ocean, 1979–2005, *Geophys. Rev. Abstr.*, *9*, 07124.

Perovich, D. K., J. A. Richter-Menge, K. F. Jones, and B. Light (2008), Sunlight, water, and ice: Extreme Arctic sea ice melt during the summer of 2007, *Geophys. Res. Lett.*, *35*, L11501, doi:10.1029/2008GL034007.

Rampal, P., J. Weiss, D. Marsan, R. Lindsay, and H. Stern (2008), Scaling properties of sea ice deformation from buoy dispersion analysis, *J. Geophys. Res.*, *113*, C03002, doi:10.1029/2007JC004143.

Richardson, L. F., and H. Stommel (1949), Note on eddy diffusion in the sea, *J. Meteorol.*, *5*, 238–240.

Richter-Menge, J., et al. (2006), State of the Arctic report, *Spec. Rep. 2952*, 36 pp., NOAA, Seattle, Wash.

Rigor, I. G., J. M. Wallace, and R. L. Colony (2002), On the response of sea ice to the Arctic Oscillation, *J. Clim.*, *15*, 2648–2663, doi:10.1175/1520-0442(2002)015<2648:ROSITT>2.0.CO;2.

Rothrock, D., D. B. Percival, and M. Wensnahan (2008), The decline in Arctic sea-ice thickness: Separating the spatial, annual, and interannual variability in a quarter century of submarine data, *J. Geophys. Res.*, *113*, C05003, doi:10.1029/2007JC004252.

Schulson, E. M. (2004), Compressive shear faults within the Arctic sea ice: Fracture on scales large and small, *J. Geophys. Res.*, *109*, C07016, doi:10.1029/2003JC002108.

Serreze, M. C., M. M. Holland, and J. Stroeve (2007), Perspectives on the Arctic's shrinking sea-ice cover, *Science*, *315*, 1533–1536, doi:10.1126/science.1139426.

Stern, H., and R. E. Moritz (2002), Sea ice kinematics and surface properties from RADARSAT synthetic aperture radar during the SHEBA drift, *J. Geophys. Res.*, *107*(C10), 8028, doi:10.1029/2000JC000472.

Stroeve, J., M. M. Holland, W. Meier, T. Scambos, and M. C. Serreze (2007), Arctic sea ice decline: Faster than forecast, *Geophys. Res. Lett.*, *34*, L09501, doi:10.1029/2007GL029703.

Stroeve, J., M. Serreze, S. Drobot, S. Gearheard, M. Holland, J. Maslanik, W. Meier, and T. Scambos (2008), Arctic sea ice extent plummets in 2007, *Eos Trans. AGU*, *89*(2), doi:10.1029/2008EO020001.

Taylor, G. I. (1921), Diffusion by continuous movements, *Proc. London Math. Soc., Ser. 2*, *20*, 196–212.

Thomas, D. (1999), The quality of sea ice velocity estimates, *J. Geophys. Res.*, *104*, 13,627–13,655, doi:10.1029/1999JC900086.

Thompson, D. W. J., and J. M. Wallace (1998), The Arctic oscillation signature in the wintertime geopotential height and temperature fields, *Geophys. Res. Lett.*, *25*, 1297–1300, doi:10.1029/98GL00950.

Thorndike, A. S. (1986), Sea ice kinematics, in *Geophysics of Sea Ice*, edited by N. Untersteiner, pp. 489–549, Plenum, New York.

Thorndike, A. S., and R. Colony (1982), Sea ice motion in response to geostrophic winds, *J. Geophys. Res.*, *87*, 5845–5852, doi:10.1029/JC087iC08p05845.

Weiss, J., E. M. Schulson, and H. Stern (2007), Sea ice rheology from in-situ, satellite and laboratory observations: Fracture and friction, *Earth Planet. Sci. Lett.*, *255*, 1–8, doi:10.1016/j.epsl.2006.11.033.

Zhang, J., D. Rothrock, and M. Steele (2000), Recent changes in Arctic sea ice: The interplay between ice dynamics and thermodynamics, *J. Clim.*, *13*, 3099–3114, doi:10.1175/1520-0442(2000)013<3099:RCIASI>2.0.CO;2.

D. Marsan, Laboratoire de Géophysique Interne et Tectonophysique, UMR5559, Université de Savoie, CNRS, F-73376 Le Bourget du Lac, France.

P. Rampal and J. Weiss, Laboratoire de Glaciologie et Géophysique de l'Environnement, UMR5183, Université Joseph Fourier, CNRS, F-38402 Saint Martin d'Hères, France. (prampal@lgge.obs.ujf-grenoble.fr)